Theory of the scrape-off layer width in inner-wall limited tokamak plasmas

2014 Nucl. Fusion 54 043003

(http://iopscience.iop.org/0029-5515/54/4/043003)

IOP Publishing | International Atomic Energy Agency Nuclear Fusion
Nucl. Fusion 54 (2014) 043003 (9pp) doi:10.1088/0029-5515/54/4/043003

Theory of the scrape-off layer width in inner-wall limited tokamak plasmas

F.D. Halpern, P. Ricci, S. Jolliet, J. Loizu and A. Mosetto

École Polytechnique Fédérale de Lausanne (EPFL), Centre de Recherches en Physique des Plasmas, CH-1015 Lausanne, Switzerland

Received 18 October 2013, revised 12 February 2014
Accepted for publication 12 February 2014
Published 10 March 2014

Abstract

We develop a predictive theory applicable to the scrape-off layer (SOL) of inner-wall limited plasmas. Using the non-linear flattening of the pressure profile as a saturation mechanism for resistive ballooning modes, we are able to demonstrate and quantify the increase of the SOL width with plasma size, connection length, plasma β, and collisionality. Individual aspects of the theory, such as saturation physics, parallel dynamics, and system size scaling, are tested and verified using non-linear, 3D flux-driven SOL turbulence simulations. Altogether, very good agreement between theory and simulation is found.

Keywords: SOL width, turbulence, tokamak, ballooning modes, limited plasmas

(Some figures may appear in colour only in the online journal)

1. Introduction

While determining the scrape-off layer (SOL) width and understanding the transport mechanisms involved in SOL profile formation are crucial issues for ITER and all future tokamak devices, a complete understanding of the subject is still needed. In recent years, for instance, it was discovered that the L-mode scaling used to calculate the ITER heat-flux width and design the inner wall [1] did not apply to the start-up phase of the discharge, when the plasma is wall-limited. Many inner-wall limited experiments were then carried out to understand how the SOL width varies with the plasma parameters [2–8].

The goal of the present paper is to address the turbulent dynamics of circular, inner-wall limited SOL plasmas, such as the proposed ITER start-up scenario, and establish a theory-based predictive capability in this simplest configuration. Our investigations concentrate on the characteristic pressure gradient length $L_p = -p/\nabla p$, which regulates the steady-state heat load on the wall. Building on recent theoretical investigations [9, 10], and complementing the initial comparison with experimental data presented in a recent letter [11], we provide a generalized analytical framework that allows us to understand the scaling of the SOL width as a function of its operational parameters. The predictions of our model are in remarkable agreement with a large simulation scan, presented here, covering a wide range of SOL parameters.

The SOL width (i.e. L_p) results from a competition between plasma outflow from the core, perpendicular transport driven by turbulent structures, and parallel losses at the end of the magnetic field lines that are determined by sheath physics. In order to address these effects, we use a global, drift-reduced Braginskii fluid model [12] in combination with a proper set of boundary conditions at the magnetic pre-sheath entrance [13]. We carry out flux-driven, global 3D simulations in circular geometry with a toroidal limiter on the equatorial plane at the high-field side. The quasi-steady-state profiles result from turbulence driven by flute-like, large amplitude meso-scale structures such as those experimentally observed.

Our main results can be summarized as follows. The saturation model proposed, in combination with a linear stability code, yields L_p within 10% of the fully non-linear computation using the SOL operational parameters only as an input. Noticing that the resistive ballooning mode (RBM) is the instability driving turbulence in the simulations, it is shown that the steady state L_p (normalized by $\rho_s = c_s/\omega_{ci} = \sqrt{T_e/m_i}/(eB/m_i)$) can be estimated using the following scaling:

$$L_p = \left[2\pi\rho_\star\alpha_d(1-\alpha)^{1/2}/q\right]^{-1/2}, \tag{1}$$

for α below the ideal ballooning threshold. The dimensionless parameters regulating the SOL width are the safety factor $q = (r/R)(B_\phi/B_\theta)$; the collisional parameter $\alpha_d = 2^{-7/4}\nu^{-1/2}(\rho_\star L_p^{-1/4})/(\pi q)$; the ideal ballooning stability parameter $\alpha = q^2\beta R/L_p$; and the normalized ion-sound gyroradius $\rho_\star = \rho_s/R$. (r and R are the tokamak minor and major radii, $\nu = e^2 nR/(m_i c_s \sigma_\|)$ is the normalized Spitzer resistivity, $\beta = 2\mu_0 p/B^2$ is the ratio of kinetic to magnetic pressure, and $\sigma_\|$ is the Spitzer conductivity. Also, note that the typical definition of $\rho_\star$ uses the minor radius a instead of R.) Our analysis of the simulation data reveals very good agreement with our analytical theory. At fixed $\rho_\star$, it is shown that the variation of the SOL width is determined by the dimensionless parameters α_d/q and α. We also analyse in detail the SOL width dependence on $\rho_\star$, discussing deviations from the RBM estimate. Finally, it is remarked that, while there have been previous attempts at understanding the SOL width scaling using 2D models [14–17], our results reveal the importance of 3D effects such as parallel resistivity and electromagnetic fluctuations in determining L_p in the SOL.

This paper is organized as follows. In section 2, the physical model used to study SOL turbulence is discussed. Then, in section 3, a theory predicting the SOL width as a function of the dimensionless parameters is derived. Section 4 describes the results of SOL non-linear turbulence simulations, which serve as a verification of our theory. We discuss and disentangle, in particular, saturation physics and the effects of parallel dynamics and system size. Section 5 presents a summary of the findings of this work.

2. Model

In the tokamak SOL, it is of particular interest to understand temperature and density profile formation, which occurs as a power balance between particle and heat injection from the plasma core, perpendicular transport driven by turbulence, and parallel losses at the sheaths where the magnetic field lines intersect the vacuum vessel. The excitation of turbulent modes can result from a combination of unfavourable magnetic field curvature, pressure gradients, and electron adiabaticity breaking either by resistivity or electron inertia effects, which can be enhanced by electromagnetic effects. The resulting turbulent dynamics is characterized by the presence of meso-scale structures, i.e. large amplitude structures with a significant radial extension.

SOL turbulence investigations must therefore be global, and flux driven; both micro (up to ρ_s) and macroscopic (L_p) length scales must be resolved, and the turbulent fluctuations cannot be formally separated from the background. Particle trapping is negligible since $\nu_\star \gg 1$ in the SOL of limited plasmas, while finite Larmor radius effects are small since $k_\theta\rho_s \sim 0.1$ for the typical dominant modes in the non-linear stage. Since the plasma is relatively cold, a fluid model can capture the essential physical ingredients of this system.

For the present study, we use a cold-ion drift-reduced model [12], which can be derived from the Braginskii two-fluid equations [18] by imposing the orderings $\mathrm{d}/\mathrm{d}t \ll \omega_{ci}$, $k_\perp \gg k_\parallel$, and $T_i \ll T_e$. The drift-reduced equations, in normalized units, read as follows:

$$\partial_t n = -\rho_\star^{-1}[\phi, n] - \nabla_\parallel\left(n v_{\parallel e}\right) + 2\left[\hat{C}(p_e) - n\hat{C}(\phi)\right] + D_n\nabla_\perp^2 n + S_n \quad (2)$$

$$\partial_t\omega = -\rho_\star^{-1}[\phi, \omega] - v_{\parallel i}\nabla_\parallel\omega + \frac{2}{n}\hat{C}(p_e) + \frac{1}{n}\nabla_\parallel j_\parallel + \frac{\hat{C}(G_i)}{3n} + D_\omega\nabla_\perp^2\omega \quad (3)$$

$$\partial_t\chi = -\rho_\star^{-1}\left[\phi, v_{\parallel e}\right] - v_{\parallel e}\nabla_\parallel v_{\parallel e} + D_{v_{\parallel e}}\nabla_\perp^2 v_{\parallel e} + \frac{m_i}{m_e}\left(\nu\frac{j_\parallel}{n} + \nabla_\parallel\phi - \frac{1}{n}\nabla_\parallel p_e - 0.71 n\nabla_\parallel T_e - \frac{2}{3n}\nabla_\parallel G_e\right) \quad (4)$$

$$\partial_t v_{\parallel i} = -\rho_\star^{-1}\left[\phi, v_{\parallel i}\right] - v_{\parallel i}\nabla_\parallel v_{\parallel i} - \frac{1}{n}\nabla_\parallel p_e - \frac{2}{3n}\nabla_\parallel G_i + D_{v_{\parallel i}}\nabla_\perp^2 v_{\parallel i} \quad (5)$$

$$\partial_t T_e = -\rho_\star^{-1}[\phi, T_e] - v_{\parallel e}\nabla_\parallel T_e + \frac{4}{3}T_e\left[\frac{7}{2}\hat{C}(T_e) + \frac{T_e}{n}\hat{C}(n) - \hat{C}(\phi)\right] + \frac{2}{3}T_e\left(\frac{0.71}{n}\nabla_\parallel j_\parallel - \nabla_\parallel v_{\parallel e}\right) + D_{T_e}\nabla_\perp^2 T_e + S_{T_e}, \quad (6)$$

where $\omega = \nabla_\perp^2\phi$ is the vorticity and equation (3) has been simplified using the Boussinesq approximation $\nabla\cdot(nd_t\nabla_\perp\phi) \approx nd_t\nabla_\perp^2\phi$. The quantity $\chi = [v_{\parallel e} + m_i\beta_0\psi/(2m_e)]$ represents a combination of inertial and induction effects in the Ohm's law, $j_\parallel = n(v_{\parallel i} - v_{\parallel e})$ is the parallel current, $\nu = e^2nR/(m_i\sigma_\parallel\bar{c}_s)$ is the normalized Spitzer resistivity, and $\beta_0 = 2\mu_0\bar{n}\bar{T}_e/B_0^2$ is the reference beta ($\bar{n}$ and $\bar{T}_e$ are, respectively, the reference electron density and temperature, and $\bar{c}_s = \sqrt{\bar{T}_e/m_i}$). Here, $\psi = -\boldsymbol{b}_0\cdot\boldsymbol{A}_1$ is the parallel component of the magnetic vector potential given by $\nabla\times\boldsymbol{A}_1 = \boldsymbol{B}_1$. The unit equilibrium magnetic field vector is $\boldsymbol{b}_0 = \boldsymbol{B}_0/B_0$ (subscripts '0' and '1' indicate equilibrium and perturbed quantities, respectively). The parallel current and the poloidal flux function are related through Ampère's equation, $\nabla_\perp^2\psi = j_\parallel$.

The following normalizations are used in the drift-reduced equations: $t = \tilde{t}/(R/\bar{c}_s)$, $\nabla_\perp = \bar{\rho}_s\tilde{\nabla}_\perp$, $\nabla_\parallel = R\tilde{\nabla}_\parallel$, $v_\parallel = \tilde{v}_\parallel/\bar{c}_s$, $n = \tilde{n}/\bar{n}$, $T_e = \tilde{T}_e/\bar{T}_e$, $\phi = e\tilde{\phi}/\bar{T}_e$, and, $\psi = \tilde{\psi}/[2\bar{c}_s m_i/(e\beta_0)]$. Here, the tildes denote quantities in MKS physical units, and the bars denote reference quantities defined in terms of the normalized density $\bar{n}$ and temperature $\bar{T}_e$. All variables are expressed in their adimensional form unless specified otherwise.

Plasma outflow from the closed flux-surface region is mimicked using density and temperature sources, respectively, S_n and S_{T_e}. The G_e and G_i terms represent the gyroviscous part of the pressure tensor (see [12]). Small perpendicular diffusion terms of the form $D_f\nabla_\perp^2 f$ are added mostly to allow the numerical solution of the system. In addition, $[f, g] = \boldsymbol{b}_0\cdot(\nabla f\times\nabla g)$ is the Poisson bracket, while $\hat{C}(f) = (B_0/2)[\nabla\times(\boldsymbol{b}_0/B_0)]\cdot\nabla f$ is the curvature operator. The parallel gradient includes the effect of perpendicular electromagnetic perturbations, and is defined as $\nabla_\parallel f = \hat{b}_0\cdot\nabla f + \beta_0\rho_\star^{-1}[\psi, f]/2$.

We consider a SOL model in circular geometry with a toroidal limiter set at the high-field-side equatorial mid-plane. The coordinate system used is (θ, r, φ), right-handed—r is the radial coordinate, with $r = 0$ set at the last closed flux surface, θ is the poloidal angle, and φ is the toroidal angle. Under these assumptions, the curvature operator reduces to $\hat{C}(f) = (\sin\theta)\partial_x f + (\cos\theta + \hat{s}\theta\sin\theta)\partial_\theta f$ and the Poisson bracket is defined as $[f, g] = a^{-1}(\partial_\theta f\partial_x g - \partial_x f\partial_\theta g)$ ($\hat{s} = (a + r)q'/q$ is the magnetic shear).

The plasma interfaces with the vacuum vessel through a magnetized pre-sheath where the fluid drift approximation breaks down. The validity of the drift-reduced model, therefore, formally extends until the magnetic pre-sheath entrance, where we apply an appropriate set of boundary conditions [13]:

$$v_{\parallel i} = \pm c_s \quad (7)$$

$$v_{\parallel e} = \pm c_s\exp\left(\Lambda - \phi/T_e\right) \quad (8)$$

$$\omega = -\cos^2\left(\frac{r}{qR}\right)\left[\left(\frac{\partial v_{\parallel i}}{\partial\theta}\right)^2 \pm c_s\frac{\partial^2 v_{\parallel i}}{\partial\theta^2}\right]a^{-2} \quad (9)$$

$$\psi = 0 \quad (10)$$

$$\frac{\partial n}{\partial \theta} = \mp \frac{n}{c_s}\frac{\partial v_{\parallel i}}{\partial \theta} \quad (11)$$

$$\frac{\partial \phi}{\partial \theta} = \mp c_s \frac{\partial v_{\parallel i}}{\partial \theta} \quad (12)$$

$$\frac{\partial T_e}{\partial \theta} = 0, \quad (13)$$

where $\Lambda \approx 3$.

Since our study discusses plasma size and quantities such as ν, q and β, which determine parallel dynamics, it is useful to discuss how these parameters enter the drift-reduced Braginskii model. The simulated plasma size is incorporated into the equations through the $\boldsymbol{E} \times \boldsymbol{B}$ flow advective terms arising from the total time derivative, which are varied through the dimensionless parameter $\rho_\star$. In our simulations, decreasing $\rho_\star$ is equivalent to increasing the toroidal magnetic field, decreasing the temperature, or increasing the machine size. In addition, the plasma size enters the equations through the normalization of the collisionality ν.

Parallel dynamics involve, on one hand, sonic flows that carry the plasma towards the plasma sheaths, and, on the other, a coupling between the vorticity equation $\nabla \cdot \boldsymbol{j} = 0$ and Ohm's law (equations (3) and (4)). The parallel flows affect mainly the bulk of the plasma and carry bulk density and heat towards the limiter where the magnetic field lines terminate (equations (2) and (6)). Since the major radius is used to normalize the parallel scale length, its value does not appear explicitly in the parallel loss terms $\sim \nabla_\parallel (p v_{\parallel e})$.

The parallel electron motion, which is coupled to the vorticity equation, is responsible for adiabaticity breaking, allowing different instabilities to grow. The effects included in the Ohm's law are the plasma resistivity, electron inertia, electromagnetic induction, and diamagnetic stabilization. This leads to our model being able to describe the resistive and inertial branches of drift waves and ballooning modes, and, in addition, the ideal ballooning mode. In the regime of interest for typical limited discharges ($\beta \sim 10^{-5}$, $0 \lesssim \hat{s} \lesssim 2$, $\nu \approx 0.005$–0.05, $3 < q < 10$), resistivity is the most important destabilization mechanism and mode growth is fed by unfavourable curvature [19].

The plasma size and parallel dynamics are instrumental in understanding the SOL width, since they affect the amplitude and dominant wavelength of the turbulent modes in the non-linear quasi-steady-state phase. Our theoretical understanding of these effects is developed below in section 3, and a large set of non-linear simulation results testing our theory are presented in section 4.

3. Theory of the SOL width

In a recent study [9], it has been shown that the magnitude of the turbulent fluxes in the SOL can be predicted using the *gradient-removal* mechanism, i.e. the local non-linear flattening of the pressure profile caused by the turbulent structures. The gradient-removal model has been used to explain experimental observations of L_p in a number of tokamaks [11], the transition between different unstable modes depending on the plasma parameters [19], the effects of finite aspect ratio [20], and the transition between the electrostatic and the ideal ballooning unstable regimes [10]. A short summary of the model follows below.

In our non-linear, flux-driven simulations, it is observed that sheared flows are unable to significantly affect the turbulence levels. Turbulent saturation, in fact, occurs when the linear drive from the background gradient is locally exhausted by the pressure non-linearity. Starting from this hypothesis, it follows that the amplitude of the turbulence can be estimated as $p_1/p_0 \sim \sigma_r/L_p$. The radial extension of the mode, $\sigma_r \approx \sqrt{L_p/k_\theta}$, is obtained from a non-local linear theory [21, 22]. Then, the leading order contribution of a continuity equation leads to an estimate of the turbulent $\boldsymbol{E} \times \boldsymbol{B}$ flux, $\Gamma = p_0\gamma/k_\theta$, where γ is the linear growth rate of the instability that dominates the non-linear dynamics. Power balance between perpendicular turbulent transport, $\partial_x \Gamma \sim \Gamma/L_p \sim p_0\gamma/(k_\theta L_p)$, and the parallel losses at the sheath, $\nabla_\parallel (p v_{\parallel e}) \sim p_0 c_{s0}/q$, results in an estimate of the profile length

$$L_p \sim \frac{q}{c_{s0}} \left(\frac{\gamma}{k_\theta}\right)_{\max}. \quad (14)$$

In the following, we will assume $c_{s0} = 1$, which corresponds to normalizing T_e to its background value. Furthermore, it is assumed that the flux is driven by a single mode that maximizes γ/k_θ, i.e. we assume that the non-linear phase is dominated by the poloidal mode that leads to the flattest pressure profile.

The steady state L_p can be predicted provided that the linear growth rate of the transport-driving mode is known. SOL turbulence in limited plasmas has been addressed with 3D electromagnetic simulations, finding that RBMs dominate the plasma dynamics [10, 23]. In the absence of poloidal periodicity, RBMs are dominant over non-linearly driven drift waves [23], and linearly unstable drift waves are damped by the magnetic shear [24]. Moreover, it is possible to estimate the non-linear regime instability using linear calculations and an estimate of the radial flux driven by each instability [19]. This calculation confirms the importance of RBMs in the SOL of limited plasmas.

We henceforth concentrate on the dynamics of RBMs and how they affect the SOL width. Using equations (2)–(6) together with equation (14), it is possible to show that the dimensionless parameters regulating the SOL width are q, $\rho_\star$, $\alpha = q^2\beta R/L_p$, and $\alpha_d = 2^{-7/4}\nu^{-1/2}(\rho_\star L_p^{-1/4})/(\pi q)$. The computation yields a dimensionless scaling, which predicts fully non-linear simulation results reasonably well. In order to obtain this result, we first simplify the two-fluid system (equations (2)–(6)) considerably. These simplifications are supported *a posteriori* by the fact that the simple model captures the principal ingredients of the non-linear steady-state. Starting from equations (2)–(6), we neglect: the ion parallel motion equation; compressibility effects and parallel couplings in the density and temperature equations; electron inertia and diamagnetic effects in Ohm's law; all diffusion and gyroviscous terms; and, finally, electromagnetic perturbations are ignored everywhere except for the left-hand-side of Ohm's law. The density and temperature equations are added to obtain an equation for the total pressure. The resulting system of equations is, essentially, a reduced MHD model describing resistive and ideal ballooning modes:

$$\frac{\partial p}{\partial t} = -\rho_\star^{-1}[\phi, p] \quad (15)$$

$$\frac{\partial \omega}{\partial t} = 2\hat{C}(p) + \nabla_\parallel j_\parallel \tag{16}$$

$$\frac{\beta_0}{2}\frac{\partial \psi}{\partial t} = \nabla_\parallel \phi + \nu j_\parallel. \tag{17}$$

The linear dispersion relation resulting from this model reads

$$\left(\gamma^2 - \gamma_b^2\right) k_\theta^2 = -\frac{\gamma}{\nu q^2}\left[1 - \alpha\left(1 - \frac{\gamma^2}{\gamma_b^2}\right)\right], \tag{18}$$

where the term on the right-hand side represents the parallel dynamics obtained from equation (17) and $\gamma_\mathrm{b} = \sqrt{2/(\rho_\star L_\mathrm{p})}$ is the reference RBM growth rate. In deriving equation (18) we have assumed $k_\parallel \sim 1/q$, $k_\perp \sim k_\theta$, and the curvature operator is assumed to take the simple form $\hat{C}(f) = \partial_\theta f$. Magnetic shear effects are neglected, since they have a weak influence on the RBM growth rate in the regime of interest [24].

Assuming $\alpha < 1$ (the ideal ballooning branch is neglected) and $\gamma^2 \ll \gamma_\mathrm{b}^2$, the gradient-removal flux estimate, $\Gamma = (\gamma/k_\theta)_\mathrm{max}$, can be obtained analytically. This is equivalent to a low β, low-frequency regime for RBMs. We start by solving the equation $\partial_{k_\theta}(\gamma/k_\theta) = 0$, which yields $k_\theta^2 = 3^{1/4}k_\mathrm{b}^2/\sqrt{2} \approx 0.93k_\mathrm{b}^2$, with $k_\mathrm{b}^2 = (1-\alpha)\nu^{-1}q^{-2}\gamma_\mathrm{b}^{-1} \propto (1-\alpha)\alpha_\mathrm{d}^2/\gamma_\mathrm{b}^2$. Note that the modes dominating the non-linear state have a wavelength that is intermediate between marginal stability and the strongly unstable regime. Therefore, it appears that it is not possible to simplify equation (18) using k_θ as an expansion parameter. The saturated growth rate is obtained by substituting k_θ into the solution of equation (18), which gives $\gamma = \gamma_\mathrm{b}/\sqrt{3} \approx 0.57\gamma_\mathrm{b}$. To obtain L_p, we use equation (14) together with the estimates $\gamma = \gamma_\mathrm{b}$ and $k_\theta = k_\mathrm{b}$, which yields a dimensionless scaling:

$$L_\mathrm{p} = \left[2\pi\rho_\star\alpha_\mathrm{d}(1-\alpha)^{1/2}/q\right]^{-1/2}. \tag{19}$$

Equation (19) clearly identifies the dimensionless parameters describing the scaling of L_p: $\rho_\star$, which describes the system size scaling; α_d/q, which includes collisional effects and the connection length; and α, which is due to electromagnetic effects. The parameters act as follows: $\rho_\star$ modifies the linear drive through γ_b; increasing α_d/q is equivalent to increasing the conductivity or decreasing the connection length, which inhibits mode growth at low k_θ; while α enhances the non-adiabatic electron response and has a destabilizing effect on the electrostatic resistive branch.

This expression for L_p is equivalent to the dimensionless scaling derived in [11] (with $\rho_\star$ being equivalent to the parameter $\tilde{R}^{-1}$ introduced therein). Additionally, note that both α_d and α include factors of L_p—therefore, equation (19) is an implicit scaling. In the low beta case, $\alpha \ll 1$, it is possible to obtain an explicit scaling as a function of the GBS input parameters $\rho_\star$, q and ν. The expression for the SOL width is

$$L_\mathrm{p} = 2^{3/7}\rho_\star^{-3/7}q^{8/7}\nu^{2/7}. \tag{20}$$

This simple theory of the SOL width, which is applicable in inner-wall limited discharges, has been fully verified against non-linear simulations describing SOL profile formation. More specifically, we have explored the effects of changing plasma size, resistivity, plasma β, and connection length separately. The non-linear simulation results are described below.

4. Non-linear simulations

We have carried out an extensive simulation campaign aiming to understand saturation physics, parallel dynamics, and plasma size effects in inner-wall limited plasmas. Global, flux-driven, non-linear simulations of the SOL dynamics are carried out with GBS [12], a numerical implementation of the global drift-reduced Braginskii model (equations (2)–(6) with boundary conditions (7)–(13)). GBS was originally developed to study turbulence in basic plasma physics experiments, and is fully validated against TORPEX probe measurements (e.g. [22, 25–28]). Since 2011, GBS is also capable of carrying out flux-driven simulations of the tokamak SOL in limited configuration. The plasma dynamics are evolved within an annulus in the open magnetic field line region of the plasma vessel. Entire flux surfaces, up to the limiter, are included in the simulation domain. We use a simple circular geometry with a toroidal limiter on the high-field side mid-plane, with constant q and constant $\hat{s}$.

In the simulated SOL dynamics, there is no separation between fluctuations and background profiles, and no length scale separation is imposed. Plasma sources, which mimic the plasma outflow from the core, increase the pressure gradient until linearly unstable modes appear, driving turbulence that leads to perpendicular transport. Over a longer period, a non-linear quasi-steady turbulent state is naturally achieved as a power balance between plasma injection, turbulent transport, and parallel losses at the plasma sheaths.

We simulate SOL plasmas where RBMs are expected to dominate transport, and we attempt to maximize the range of the dimensionless parameter space probed. We use $q = \{3, 4, 6\}$, $\nu = \{0.01, 0.1, 1\}$, $m_\mathrm{i}/m_\mathrm{e} = 200$ and $\beta_0 = 0$–3×10^{-3}. The normalized plasma sizes used were $\rho_\star = \{500, 1000, 2000\}^{-1}$, with an aspect ratio $R/a = 4$. In the plasma size scan we used $\hat{s} = 0, 1$. Note that, since GBS simulations are global, the simulation domain size must be increased with $\rho_\star^{-1}$, resulting in significant use of high-performance computing resources. The pressure profiles observed in the turbulent steady-state typically have the form $p \sim \exp(-r/L_\mathrm{p})$ with L_p ranging from 25 to 150.

In the subsections below we deal specifically with the different aspects of our SOL width theory (section 3). The saturation model is investigated in the context of non-linear simulations in section 4.1. Then, in section 4.2, the theory-based scaling is directly compared against a scaling obtained from the simulation results. The parallel dynamics effects (q, α, and α_d) and the system size scaling effects ($\rho_\star$) are studied in sections 4.3 and 4.4, respectively.

4.1. Saturation mechanism

Here, we present a verification of the *gradient-removal* model using the simulation database described above. To that effect, we implement an iterative scheme to solve equation (14). With the SOL dimensionless operational parameters $\rho_\star$, q, ν, β_e, and $\hat{s}$ fixed, the linear growth rate γ is computed using a drift-Braginskii linear solver [24] and L_p is varied iteratively until equation (14) is satisfied. It is remarked that γ is a function of the plasma parameters L_p, k_θ, $\rho_\star$, q, ν, β_0, $\hat{s}$, while the obtained result is L_p as a function of $\rho_\star$, q, ν, β_0, and $\hat{s}$.

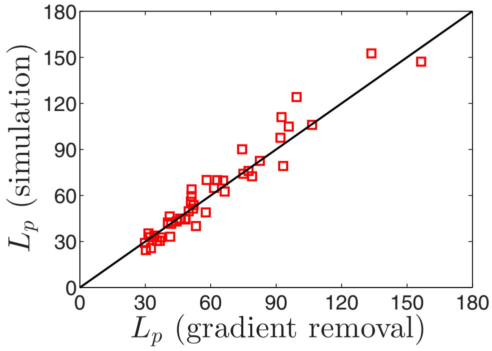

Figure 1. The gradient-removal estimate for L_p is compared against GBS non-linear simulations of SOL turbulence. The coefficient of determination given by gradient-removal theory is $R^2 \approx 0.93$.

The result of the computation is the value of L_p that satisfies the power balance between perpendicular transport and parallel losses at the field line ends, for a set of SOL operational parameters.

This procedure was carried out for all the simulations described in this paper. The results of the verification exercise are shown in figure 1. The abscissa shows the theoretical prediction provided by equation (14) while the ordinate shows the GBS fully non-linear result. Overall, very good agreement is found throughout the entire parameter range, with a coefficient of determination $R^2 \approx 0.93$. By providing an explanation of the power balance, gradient-removal theory gives an interpretation for the different physical effects involved in setting the SOL width.

The saturation mechanism, when applied to the RBM, yields the dimensionless scaling given by equation (19). We have verified this scaling against non-linear simulations with $\alpha \lesssim 0.5$, which is necessary in order to avoid ideal instability. This low β regime is, in fact, the experimentally relevant scenario for inner-wall limited discharges. The results of the comparison are shown in figure 2, where the abscissa provides the analytical scaling estimate, while the ordinate provides the fully non-linear L_p. There is relatively good agreement between theory and simulations for a large range of parameters, with a coefficient of determination for the fit of $R^2 \approx 0.72$.

Finally, since the gradient-removal computation also yields the expected non-linear value of k_θ, it is worth commenting on this issue. We have found that the peak k_θ of the non-linear simulations increases with α_d and decreases with $\gamma_\mathrm{b} \sim \rho_\star^{-1/2}$. This is exactly what is expected from the RBM theory, since $k_\mathrm{b} \propto \alpha_\mathrm{d}/\gamma_\mathrm{b}$. However, the non-linear turbulent spectra are rather wide, with a full-width half-maximum $\Delta k_\theta \sim k_\theta$. Therefore, a detailed quantitative comparison between theory and simulations (e.g. such as figure 1) is not possible.

4.2. Comparison with non-linear regression analysis of simulation data

In addition to the theoretical scaling, equation (19), it is also possible to obtain a dimensionless SOL width scaling by carrying out a least-squares fit on the simulation data. We have carried out this exercise, which also serves as a verification of our theory. All simulations in the scan are included, provided that they reside below the ideal stability threshold.

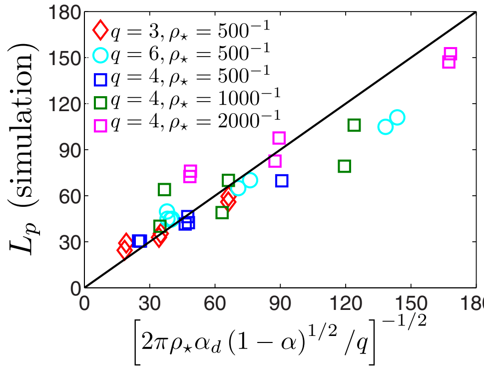

Figure 2. GBS turbulence simulation results are compared with the analytical scaling of the SOL width (equation (19)) as a function of the dimensionless parameters $\rho_\star$, α and α_d/q. The coefficient of determination for the fit is $R^2 \approx 0.72$.

The least-squares fit based on the dimensionless parameters q, $\rho_\star$, α_d, and α gives

$$L_\mathrm{p} = 0.42\, q^{0.55} \rho_\star^{-0.53} \alpha_\mathrm{d}^{-0.32} \left(1-\alpha\right)^{-0.24}. \qquad (21)$$

The coefficient of determination resulting from this fit is $R^2 \approx 0.94$. Note that the exponents and even the numerical constant of equation (21) are very similar to the ones found in equation (19). With the exception of the α_d (collisional) dependence, all exponents are within 10% of the theoretical results.

On the other hand, the fit based on the GBS parameters q, $\rho_\star$, ν and β_0 is

$$L_\mathrm{p} = 1.00\, q^{0.98} \rho_\star^{-0.46} \nu^{0.17} \beta_0^{0}, \qquad (22)$$

which then leads to an MKSA scaling of the form

$$L_\mathrm{p} \sim q^{0.98} R^{0.63} B^{-0.56}, \qquad (23)$$

with weak dependences on density and temperature, i.e. essentially the same scaling found in our recent letter [11] and reported in equation (20) using only theoretical arguments.

We have investigated the difference between the collisionality dependences found in the theory ($L_\mathrm{p} \sim \nu^{2/7}$) and in the simulations. We employ the quasi-linear, self-consistent computation of L_p described in section 4.1 at fixed $R = 500$, $q = 4$, and varying ν. The result is that the ν exponent is affected (a) by the use of an increased electron mass in the GBS simulations and (b) by the assumption of full non-adiabaticity in equation (17). Therefore, the assumptions used to deduce the RBM scaling are not fully satisfied in our simulations.

4.3. Parallel dynamics

Here, we investigate the effects of the dimensionless parameters describing the SOL parallel dynamics. Our objective is to build a SOL dimensionless parameter space describing collisional and finite β effects, verifying that α, and α_d/q are indeed the relevant dimensionless parameters. The SOL width L_p and the dimensionless parameters suggested by equation (19), α_d and α, are computed using equation (14) together with the linear growth rate provided by the drift-Braginskii linear solver [24]. The following parameter

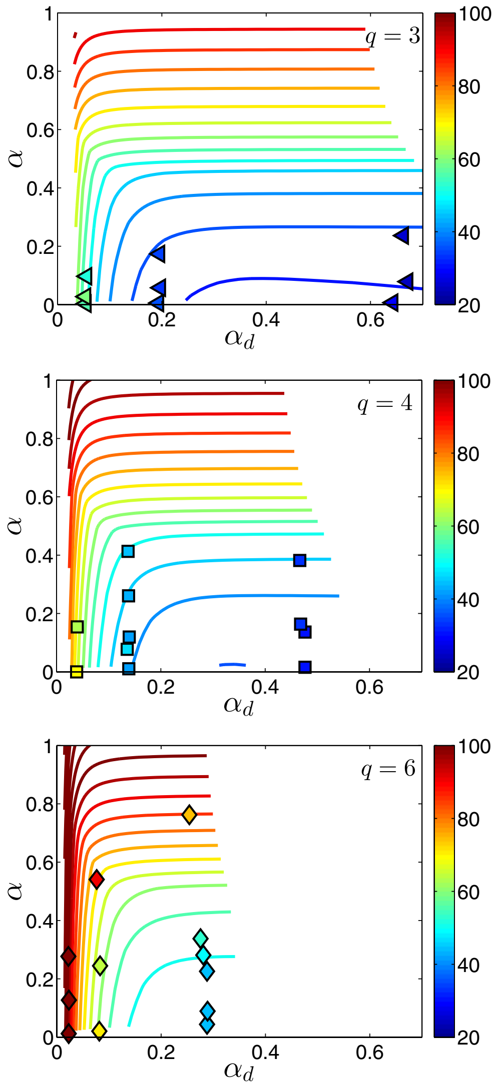

Figure 3. Gradient length is shown as a function of α and $\alpha_{\rm d}$ for $q = 3, 4$ and 6. The coloured contours indicate $L_{\rm p}$ predicted by equation (14), while each symbol represents a non-linear simulation. Triangles represent simulations with $q = 3$, squares simulations with $q = 4$, and diamonds simulations with $q = 6$.

space was explored: $\rho_\star = 500^{-1}$, $\hat{s} = 0$, $q = 3, 4, 6$, $\nu = 0.01$–1, $\beta_0 < 10^{-2}$. The resulting dimensionless parameter spaces for $q = 3$, 4, and 6 are displayed in figure 3, where we show contours of equal $L_{\rm p}$ with non-linear simulation results superimposed showing good agreement. It is observed that the dimensionless parameter space covered is different in each case, as both α and $\alpha_{\rm d}$ depend on q. High q values naturally result in a wider SOL through a combination of increased resistive ($\alpha_{\rm d}$) and electromagnetic (α) effects. The calculation confirms the interpretation obtained starting from equation (18), i.e. $L_{\rm p}$ increases in the regime where we predicted destabilization of resistive modes from low $\alpha_{\rm d}$ (a combination of high resistivity and long connection length), and increasing α (increased non-adiabatic electron response through electromagnetic perturbations).

Based on these results, and provided that the SOL dynamics are given by gradient-removal saturated RBMs, we now establish a unified dimensionless parameter space that is valid for any value of q. Equation (19) suggests that the dimensionless parameter space is given by α and $\alpha_{\rm d}/q$. In figure 4, we plot the $L_{\rm p}$ contours for $q = 4$ as a function of these two parameters. We have superimposed the GBS simulation data obtained for all the simulations with $\rho_\star^{-1} = 500$, for all of the q values. The theoretical model yields a good prediction of the values of $L_{\rm p}$ obtained in non-linear simulations, with $L_{\rm p}$ often being predicted within $5\rho_{\rm s}$. Note that the relevant dimensionless parameter describing resistive and connection length effects is therefore $\alpha_{\rm d}/q$ and not $\alpha_{\rm d}$ itself.

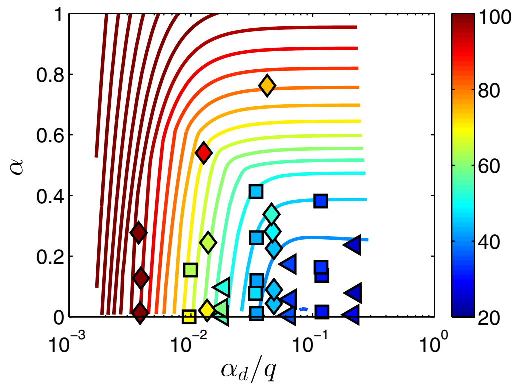

Figure 4. Unified dimensionless electromagnetic parameter space built using gradient-removal theory in combination with the fluid linear system. Here $L_{\rm p}$ is shown as a function of α and $\alpha_{\rm d}/q$. The coloured contours indicate $L_{\rm p}$ predicted by equation (14), while each symbol represents a non-linear simulation. Triangles represent simulations with $q = 3$, squares simulations with $q = 4$, and diamonds simulations with $q = 6$.

These dimensionless parameters, which we propose for the SOL of *limited* discharges, may not apply to the SOL of *diverted* discharges. In Alcator C-Mod, for example, it has been shown that the relevant dimensionless parameters for the near SOL are $\alpha_{\rm d}$ and α [29, 30]. In particular, it was demonstrated that $L_{\rm p}$ decreases with decreasing $\alpha_{\rm d}$ and, furthermore, it was observed that $\alpha_{\rm d}$ and α both decrease as the Greenwald density limit is approached.

4.4. Plasma size scaling

The variation of $L_{\rm p}$ with system size is one of the greatest uncertainties that must be resolved as we approach the era of ITER ($\rho_\star \sim 10^{-4}$, which is impractical to simulate at the present time). We have carried out a set of simulations that address the system size scaling of the SOL width in limited plasmas such as the proposed ITER start-up scenario. In order to understand $\rho_\star$ effects, we have chosen to decrease $\rho_\star$ while leaving the normalized collisionality ν and the injected power per unit volume unchanged. This is equivalent to increasing the strength of the magnetic field at fixed temperature and system size.

We start with the parameters $\rho_\star = 500^{-1}$, $q = 4$, $\nu = 0.01, 0.1, 1$, $\hat{s} = 0, 1, 2$, and increase the plasma size to $\rho_\star = 1000^{-1}$ and $\rho_\star = 2000^{-1}$. We consider the electrostatic limit, $\beta \ll 1$. The smallest simulated plasma size ($\rho_\star = 500^{-1}$) was used above to explore the parallel dynamics effects; the second size, $\rho_\star = 1000^{-1}$, is roughly equivalent to the CASTOR tokamak [31]; while $\rho_\star = 2000^{-1}$ has similar physical parameters as the SOL of TCV in limited

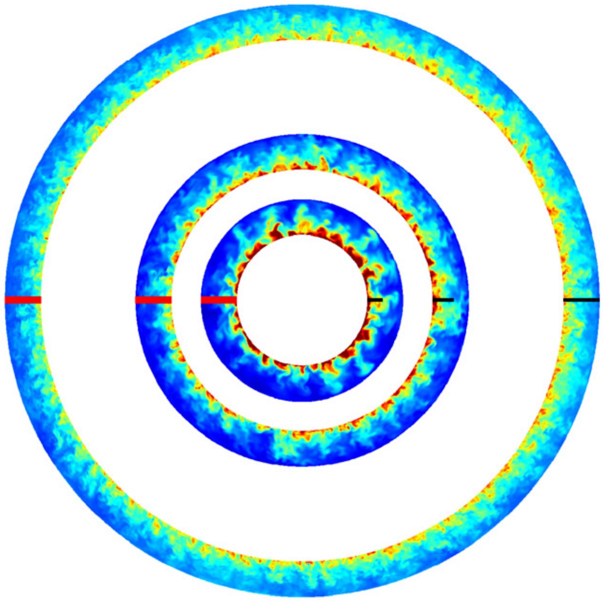

Figure 5. Poloidal cross sections of p are shown for GBS simulations with $q = 4$, $\hat{s} = 0$ and $\nu = 0.01$ as the dimensionless plasma size is increased, $\rho_\star = \{500, 1000, 2000\}^{-1}$. Note how L_p, indicated as a black line on the low-field-side equatorial mid-plane, increases as $\rho_\star$ decreases. The red bar on the high-field-side mid-plane represents the limiter. The largest case shown here has physical parameters equivalent to the TCV SOL, $R = 0.85$ m, $a = 0.2$ m, $B = 1.4$ T, $\bar{T}_\mathrm{e} = 15$ eV.

configuration [32]. In fact, for TCV ($R = 0.88$ m, $B = 1.4$ T, $\bar{T}_\mathrm{e} \approx 15$ eV, $\bar{n} \approx 3 \times 10^{18}\,\mathrm{m}^{-3}$) we obtain $\rho_\star \approx 2000^{-1}$, $\nu \approx 0.01$, $\alpha_\mathrm{d} \approx 0.5$, $\beta \approx 10^{-5}$, while $q = 3$–6 and $\hat{s} \approx 2$. The SOL of limited discharges has an experimental width of a few centimetres, $L_\mathrm{p} \sim 100$, $R/L_\mathrm{p} \approx 20$.

As an example, the quasi-steady state poloidal cross sections of the pressure for these simulations are shown in figure 5. The high-field side toroidal limiter is denoted by a red bar on the equatorial mid-plane. The profile lengths increase noticeably as $\rho_\star$ decreases ($L_\mathrm{p} = 30, 40, 72$ for $\rho_\star = \{500, 1000, 2000\}^{-1}$ respectively, and $\nu = 0.01$), in accordance to the prediction of the analytical model (equation (19)). It has also been checked that the effect of varying $\hat{s}$ from 0 to 2 at $\rho_\star = 2000^{-1}$ does not change L_p significantly, in agreement with a quasi-linear analysis assuming gradient-removal saturated turbulence [19].

It is interesting to investigate the nature of the turbulent structures in experimentally relevant parameters. We have computed the phase between the electrostatic potential and the pressure fluctuations as a function of the poloidal wavenumber k_θ. In addition, we have calculated the cross-coherence function between potential and pressure fluctuations. The results of these diagnostics are shown in figure 6 for simulations with $\rho_\star^{-1} = 2000$, $\nu = 0.01$, $\hat{s} = 0, 1, 2$ (top, centre, and bottom rows, respectively). Our diagnostic shows that the turbulent modes peak roughly at $k_\theta \approx 0.1$ for all the plasma sizes studied. Using the physical parameters corresponding to the TCV SOL, this is equivalent to a half-centimetre poloidal wavelength. The phase difference between ϕ and p_e is significant in all cases, but slightly smaller than the $\pi/2$ phase expected from the reduced MHD model leading to equation (18). The cross-coherence function shows some correlation between potential and pressure fluctuations, which decreases as $\hat{s}$ increases. The decreased phase lag and the correlation observed between ϕ and p_e perturbations are a consequence of the adiabatic electron pressure response in the Ohm's law. This effect is not taken into account in equation (18). Altogether, the mode appears to be of the ballooning kind with the resistivity providing the destabilization mechanism. We therefore confirm the importance of RBMs in limited SOL plasmas at experimentally relevant parameters. It is noted, however, that diamagnetic effects do play a role in the dynamics, in particular by weakening the non-adiabatic parallel electron response.

Finally, we estimate how L_p scales with $\rho_\star$ at fixed normalized collisionality ν. Figure 7 shows L_p from GBS simulations as a function of $\rho_\star$. The gradient-removal estimates of L_p, obtained by solving equation (14) as a function of the SOL parameters, are superimposed as lines. Once again, the saturation theory provides a reasonably good prediction of the non-linear quasi-steady-state L_p. The gradient-removal estimate for $\nu = 0.01$ follows the size scaling $L_\mathrm{p} \sim \rho_\star^{-0.57}$, while our analytical theory gives a slightly different scaling, $L_\mathrm{p} \sim \rho_\star^{-3/7} \approx \rho_\star^{-0.43}$. A more detailed quasi-linear analysis has revealed that the difference between the scalings originates from a combination of effects. On the one hand, the use of $m_\mathrm{i}/m_\mathrm{e} = 200$ slightly exaggerates the $\rho_\star$ dependence in the gradient-removal solution. On the other hand, the neglect of compressibility terms and (especially) the adiabatic electron response in the Ohm's law in deriving equation (18) weakens the $\rho_\star$ dependence with respect to the full model. This finding supports our statement that the dominant non-linear modes are RBMs with the resistive response slightly weakened by diamagnetic effects.

5. Summary and conclusions

In conclusion, we have developed and verified a theory for the SOL width of inner-wall limited plasmas. The dimensionless parameters regulating the SOL width have been identified and the effects of parallel dynamics and plasma size have been explored with the aid of large scale numerical simulations. The GBS code was used to explore a large portion of the dimensionless parameter space, including experimentally relevant physical parameters.

First, we studied the mechanism responsible for setting the amplitude of the turbulent structures. It was found that sheared flows are rather weak in our simulations. Consequently, the turbulent amplitude is limited by the local non-linear flattening of the pressure profile. From the pressure continuity equation (a power-balance relation), we can compute the expected L_p as a function of the SOL operational parameters only. Overall, excellent agreement between theory and simulation is observed for all the simulations in our large database.

Second, we have clarified the importance of parallel dynamics in setting the SOL width. Assuming that RBMs drive the perpendicular transport, and applying the gradient-removal theory, it was shown that, in limited plasmas, L_p is governed by the parameters α_d/q and α, in good agreement with GBS simulation results. These dimensionless parameters

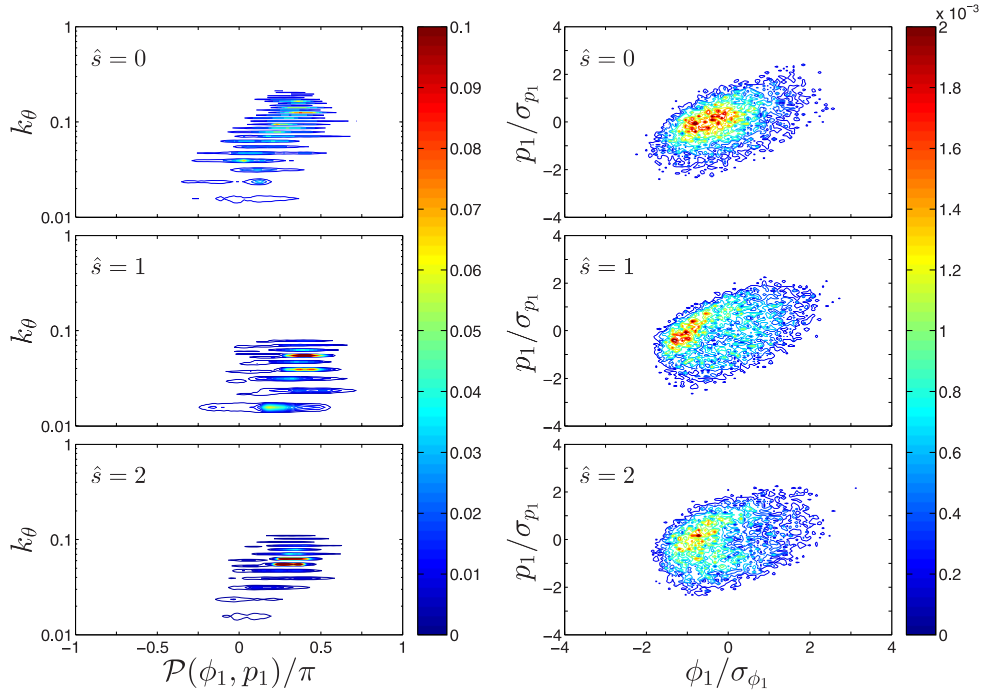

Figure 6. Phase difference (left) and cross-correlation (right) between ϕ and p_e perturbations are shown for GBS simulations with $q = 4$, $\nu = 0.01$, $\rho_\star = 2000^{-1}$, $\hat{s} = 0, 1, 2$ (top, centre, and bottom rows, respectively). The phase diagram has been renormalized using the power spectrum of the ϕ fluctuations. The cross-correlation diagram involves the distribution functions of the perturbations rescaled using their standard deviation (σ).

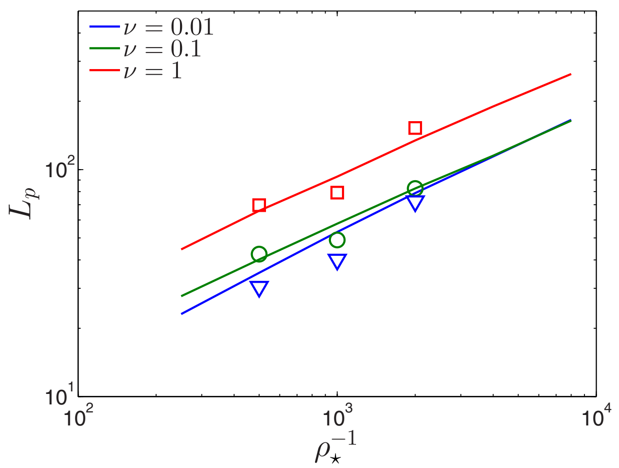

Figure 7. The pressure gradient length L_p calculated from GBS simulations with $q = 4$, $\hat{s}$ and $\rho_\star^{-1} = 500, 1000, 2000$ are shown as triangles ($\nu = 0.01$), circles ($\nu = 0.1$) and squares ($\nu = 1$). We superimpose the predictions of the *gradient-removal* theory, shown as lines. The profile length at $\nu = 0.01$ scales like $L_p \sim \rho_\star^{-0.57}$, while the analytical theory (equation (19)) predicted $L_p \sim \rho_\star^{-0.43}$.

can be used to express the SOL width in dimensionless units:

$$L_p = \left[2\pi\rho_\star\alpha_d (1-\alpha)^{1/2}/q\right]^{-1/2} \tag{24}$$

We note that the electromagnetic parameter space found (e.g. figure 4) is different respect to what has been observed for *diverted* L-mode discharges in C-Mod. In this configuration, LaBombard *et al* [29, 30] found that the relevant dimensionless parameters are α_d and α. It is conjectured that a different saturation mechanism could be at play in diverted shots. In particular, the connection length (the safety factor q) becomes very large near the X-point, and in such cases we expect Kelvin–Helmholtz modes to become important in the turbulent saturation process [9].

We also explored the effects of increasing the ‘plasma size’, more specifically, decreasing $\rho_\star$ towards experimentally relevant levels. Strictly speaking, the scan carried out in this paper is equivalent to keeping the physical plasma size, temperature, and normalized collisionality constant, while varying the toroidal magnetic field. The GBS simulations have parameters equivalent to the TCV SOL at one-quarter, one-half, and full toroidal magnetic field strength. The pressure gradient length found in the GBS simulations was found to approximately scale with size like $\rho_\star^{-0.57}$, while our analytical theory predicted a slightly weaker scaling $L_p \sim \rho_\star^{-3/7}$. The difference in exponents is due to a combination of effects (compressibility effects and adiabatic electron response) which are neglected in the derivation of equation (18). We have also confirmed that RBMs are relevant in the non-linear turbulent state at realistic SOL parameters. Our scaling, as shown in our recent letter [11], predicts $L_p \approx 6$–10 cm with $q = 6$–8 during the start-up phase of ITER.

Finally, it is suggested that, in order to reproduce our α_d scaling using 2D turbulence simulations of SOL transport, the closure of the parallel current in the vorticity equation could be modified to include a resistive damping term. Using such approach, however, it may be very challenging to model electromagnetic effects—this is particularly true in diverted configurations, where electromagnetic fluctuations are expected to be important [29, 30]. Overall, our study once again remarks the importance of retaining 3D effects, a global domain, and a full power-balance in understanding SOL profile formation—the properties of the turbulent structures, and consequently the resulting profiles, are strongly affected by the parallel dynamics, with the result that the SOL width scales favourably with plasma size.

Acknowledgments

We acknowledge useful discussions with I. Furno, B. Labit, B. Rogers and T.-M. Tran. Part of the simulations presented herein were carried out at the Swiss National Supercomputing Centre (CSCS) under project ID s346; and part were carried out using the HELIOS supercomputer system at Computational Simulation Centre of International Fusion Energy Research Centre (IFERC-CSC), Aomori, Japan, under the Broader Approach collaboration between Euratom and Japan, implemented by Fusion for Energy and JAEA. This research was supported by the Swiss National Science Foundation.

References

[1] Loarte A. *et al*, the ITPA Scrape-off Layer and Divertor Physics Topical Group 2007 Chapter 4: Power and particle control *Nucl. Fusion* **47** S203

[2] Zweben S.J., Scott B.D., Terry J.L., LaBombard B., Hughes J.W. and Stotler D.P. 2009 Comparison of scrape-off layer turbulence in Alcator C-Mod with three dimensional gyrofluid computations *Phys. Plasmas* **16** 082505

[3] Kočan M. and Gunn J.P. 2010 Comparison of scrape-off layer profiles in outboard-versus inboard-limited plasmas in Tore Supra *Plasma Phys. Control. Fusion* **52** 045010

[4] Kočan M. *et al* 2011 Measurements of ion energies in the tokamak plasma boundary *Proc. 19th Int. Conf. on Plasma–Surface Interactions in Controlled Fusion (San Diego, USA, 24–28 May 2010)*; *J. Nucl. Mater.* **415** (Suppl. 1) S1133–8

[5] Makowski M.A. *et al* 2012 Analysis of a multi-machine database on divertor heat fluxes *Phys. Plasmas* **19** 056122

[6] Gunn J.P. *et al* 2013 Scrape-off layer power flux measurements in the Tore Supra tokamak *Proc. 20th Int. Conf. on Plasma–Surface Interactions in Controlled Fusion Devices (Aachen, Germany, 21–25 May 2012)*; *J. Nucl. Mater.* **438** (Suppl. 0) S184–8

[7] Silva C., Arnoux G., Devaux S., Frigione D., Groth M., Horacek J., Lomas P.J., Marsen S., Matthews G. and Pitts R.A. 2013 Comparison of scrape-off layer transport in inner and outer wall limited JET plasmas *Proc. 20th Int. Conf. on Plasma–Surface Interactions in Controlled Fusion Devices (Aachen, Germany, 21–25 May 2012)*; *J. Nucl. Mater.* **438** (Suppl. 0) S189–93

[8] Arnoux G. *et al* and JET-EFDA Contributors 2013 Scrape-off layer properties of ITER-like limiter start-up plasmas in JET *Nucl. Fusion* **53** 073016

[9] Ricci P. and Rogers B.N. 2013 Plasma turbulence in the scrape-off layer of tokamak devices *Phys. Plasmas* **20** 010702

[10] Halpern F.D., Jolliet S., Loizu J., Mosetto A. and Ricci P. 2013 Ideal ballooning modes in the tokamak scrape-off layer *Phys. Plasmas* **20** 052306

[11] Halpern F.D. *et al* and JET-EFDA Contributors 2013 Theory-based scaling of the SOL width in circular limited tokamak plasmas *Nucl. Fusion* **53** 122001

[12] Ricci P, Halpern F.D., Jolliet S., Loizu J., Mosetto A., Fasoli A., Furno I. and Theiler C. 2012 Simulation of plasma turbulence in scrape-off layer conditions: the GBS code, simulation results and code validation *Plasma Phys. Control. Fusion* **54** 124047

[13] Loizu J., Ricci P., Halpern F.D. and Jolliet S. 2012 Boundary conditions for plasma fluid models at the magnetic presheath entrance *Phys. Plasmas* **19** 122307

[14] Sarazin Y. *et al* 2003 Theoretical understanding of turbulent transport in the SOL *J. Nucl. Mater.* **313** 796–803

[15] Garcia O.E., Horacek J., Pitts R.A., Nielsen A.H., Fundamenski W., Naulin V. and Juul Rasmussen J. 2007 Fluctuations and transport in the TCV scrape-off layer *Nucl. Fusion* **47** 667

[16] Myra J.R. *et al* and the NSTX Team 2011 Reduced model simulations of the scrape-off-layer heat-flux width and comparison with experiment *Phys. Plasmas* **18** 012305

[17] Militello F., Naulin V. and Nielsen A.H. 2013 Numerical scalings of the decay lengths in the scrape-off layer *Plasma Phys. Control. Fusion* **55** 074010

[18] Braginskii S.I. 1965 *Transport Processes in a Plasma* (*Reviews of Plasma Physics* vol 1) (New York: Consultants Bureau)

[19] Mosetto A., Halpern F.D., Jolliet S., Loizu J. and Ricci P. 2013 Turbulent regimes in the tokamak scrape-off layer *Phys. Plasmas* **20** 092308

[20] Jolliet S. *et al* 2014 Aspect ratio effects on limited scrape-off layer plasma turbulence *Phys. Plasmas* **21** 022303

[21] Rogers B.N. and Dorland W. 2005 Noncurvature-driven modes in a transport barrier *Phys. Plasmas* **12** 062511

[22] Ricci P., Rogers B.N. and Brunner S. 2008 High- and low-confinement modes in simple magnetized toroidal plasmas *Phys. Rev. Lett.* **100** 225002

[23] Ribeiro T.T. and Scott B. 2008 Gyrofluid turbulence studies of the effect of the poloidal position of an axisymmetric debye sheath *Plasma Phys. Control. Fusion* **50** 055007

[24] Mosetto A., Halpern F.D., Jolliet S. and Ricci P. 2012 Low-frequency linear-mode regimes in the tokamak scrape-off layer *Phys. Plasmas* **19** 112103

[25] Ricci P. and Rogers B.N. 2009 Transport scaling in interchange-driven toroidal plasmas *Phys. Plasmas* **16** 062303

[26] Ricci P., Theiler C., Fasoli A., Furno I., Labit B., Muller S.H., Podesta M. and Poli F.M. 2009 Langmuir probe-based observables for plasma-turbulence code validation and application to the TORPEX basic plasma physics experiment *Phys. Plasmas* **16** 055703

[27] Ricci P. and Rogers B.N. 2010 Turbulence phase space in simple magnetized toroidal plasmas *Phys. Rev. Lett.* **104** 145001

[28] Ricci P., Theiler C., Fasoli A., Furno I., Gustafson K., Iraji D. and Loizu J. 2011 Methodology for turbulence code validation: quantification of simulation-experiment agreement and application to the TORPEX experiment *Phys. Plasmas* **18** 032109

[29] LaBombard B., Hughes J.W., Mossessian D., Greenwald M., Lipschultz B., Terry J.L. and the Alcator C-Mod Team 2005 Evidence for electromagnetic fluid drift turbulence controlling the edge plasma state in the Alcator C-Mod tokamak *Nucl. Fusion* **45** 1658

[30] LaBombard B. *et al* and the Alcator C-Mod Team 2008 Critical gradients and plasma flows in the edge plasma of Alcator C-Mod *Phys. Plasmas* **15** 056106

[31] Devynck P. *et al* 2005 Spatially resolved characterization of electrostatic fluctuations in the scrape-off layer of the CASTOR tokamak *Plasma Phys. Control. Fusion* **47** 269

[32] Horacek J. 2006 Measurement of edge electrostatic turbulence in the TCV tokamak plasma boundary *PhD Thesis* N0 3524, École Polytechnique Fédérale de Lausanne, Lausanne, 2006